

Theoretical and Experimental Study of Some Parameters of Solar Drying of Fresh Vegetables, Case of Tomatoes, In South-West Algeria

Mana Saadeddine^{1,2}, Didiche Hana¹

¹ Hydrocarbon and Renewable Energy Department, Science and Technology Faculty,
Ahmed Draia University - Adrar – ALGERIA

² Mechanical Engineering Department, University of Biskra, Biskra-ALGERIA

Abstract: *Our present work is a theoretical and experimental study of solar drying of fresh tomatoes produced in the region of Adrar. The present work is a theoretical and experimental study of solar drying of fresh tomatoes produced in the city of Adrar. Through this study, we have experimentally determined the evolution of the drying kinetics as a function of several operating parameters, the drying air and the quantity of dried product, in order to establish the best conditions for indirect solar drying in the climatic conditions of this part of the great Algerian south.*

Keywords: Solar, dryer, performance, vegetable, quality

1. Introduction

Solar deposits are among the non-polluting and economical sources of energy that are increasingly in demand at the international level. Despite its importance, solar energy remains little exploited in the countries of the South, particularly in Algeria.

The drying of fruit and vegetables is one of the oldest methods of food preservation known to man. The main purpose of drying agricultural products is to reduce the moisture content to a level that allows safe storage for a long period. It also reduces weight and volume, which reduces packaging, storage and transport costs [1].

Many scientists have studied the modelling of solar drying of agricultural products and there are also simulations of studies on solar dryers and the behaviour of various vegetables and fruits, characterised by the drying kinetics. It is always difficult to control the drying process without simplifying assumptions.

2. Materials and methods

2.1. Description of the Drying System

The device used is shown in fig.1, it is an indirect solar dryer that can work in forced or natural convection, it is composed of two main parts: a flat solar collector that serves to heat the air and a parallelepiped drying room [1]. The product to be dried will be placed on the six (06) racks (dimensions: $L_c=0.950m$, $l_c=0.850m$, with a total drying surface of $4.845 m^2$).



Fig. 1: Indirect solar dryer with forced and natural convection

2.2. Experimental Protocol

All the experimental work is carried out in the city of Adrar, which is located in south-west Algeria, Longitude: -0°28 E, Latitude: 27°88 S, Altitude: 264 m.

Before drying, the tomatoes are well cleaned with clear water, then they are cut in slices of 10, 15 and 20 mm thickness and then they are placed on racks in the drying chamber with the same weights.

2.3. Drying Characteristic Curve

The concept of the characteristic drying curve was developed by Van Meel in 1957 [1]. The aim is to model the drying rate, to examine whether it is possible to obtain at the macroscopic level certain simplicity of interpretation of the experimental results [1-3], the same pattern of product behaviour is studied, whatever the conditions of the experiment.

The approach consists of normalising the average water contents and drying speeds to obtain a single curve for a given product, of given dimensions and independently of the aero thermal conditions [1], [4]. This concept of characteristic drying curve has been taken up by J. Van Brakel [5]. The implementation of the drying characteristic curve concept requires the use of certain form correlations:

The water content, normalized or reduced X^* expressed by:

$$X^* = \frac{X(t) - X_{eq}}{X_{cri} - X_{eq}} \quad (1)$$

The water content at equilibrium corresponds to the limit value obtained after an infinite time for a product subjected to given conditions of temperature and humidity.

The drying rate $(-dX/dt)$ is normalized and reduced by the rate of the first phase $(-dX/dt)_0 = \text{cst}$, which can either be deduced theoretically or measured directly from the experimental curve $-dX/dt = f(X)$, so that:

$$\left(-\frac{dX}{dt}\right) / \left(-\frac{dX}{dt}\right)_0 = \frac{h_0 S_0 \Delta T}{m_s \cdot L_v (T_h)} \quad (2)$$

The drying characteristic curve is then obtained by plotting the curve:

$$\frac{-\frac{dX}{dt}}{(T_s - T_h) \cdot (V_a)^{0.5}} = f(X^*) \quad (3)$$

The mathematical modelling of the drying curves was carried out on the basis of the mathematical models presented in Table 1.

TABLE I: Mathematical models of solar drying curves

Model	Equation
Newton	$X_r = e^{-at}$
Henderson and Pabis	$X_r = a e^{-bt}$
Henderson and Pabis modified	$X_r = a e^{-bt} + c e^{-dt} + d e^{-ft}$
Logarithmic	$X_r = a e^{-bt} + c$
Two terms	$X_r = a e^{-bt} + c e^{-dt}$
Wang and Singh	$X_r = 1 + a t + b t^2$
Parabolic	$X_r = a + b t + c t^2$

2.4. Estimation of Mass Diffusivity and Activation Energy

The transfer of moisture during drying is controlled by internal diffusion. Fick's second law of diffusion has been widely used to describe the drying process of most organic products. The solution to Fick's second law proposed by Crank is [6], [7]:

$$\frac{M - M_e}{M_0 - M_e} = \frac{8}{\pi^2} \sum_{n=1}^{\infty} \frac{1}{2n+1} e^{\left[-(2n-1)^2 \frac{\pi^2 D t}{4 L^2}\right]} \quad (4)$$

The solution takes into account the initial water content (M_0), the water content at equilibrium (M_e) and the thickness of the sample (L). Simplifying equation (3) by taking the first term of the standard solution and assuming M_e equal to 0 [9]:

$$MR = \frac{M}{M_0} = \frac{8}{\pi^2} e^{\left[\frac{\pi^2 Dt}{4 L^2} \right]} \quad (5)$$

Since drying occurs only on one surface of the sample, the thickness L in equations (3) and (4) is replaced by $(L/2)$. The thin film equation used by Zogzas [7] is:

$$-\frac{dM}{dt} = K(M - M_e) \quad (6)$$

With K is the drying constant. By comparing equations (2) and (3) [8-9], the drying constant (K) can be approximated to the mass diffusivity by the following relation [7]:

$$K = \frac{\pi^2 D}{L^2} \quad (7)$$

The relationship between temperature and mass diffusivity follows the Arrhenius expression [9]:

$$D = D_0 \cdot e^{\left(-\frac{E_a}{RT} \right)} \quad (8)$$

3. Results and Discussions

3.1. Calculation of Solar Radiation Received

The studies, which are the subject of the influence of direct and diffuse radiation on the performance of the planar sensors, have shown that the underestimation of diffuse radiation is unacceptable when their percentage is above 15%. This is explained by the fact that a high percentage of diffuses corresponds to a low energy illumination and subsequently the little energy available is received by a low efficiency sensor.

The incident solar radiation (I_g) received on a solar collector inclined at an angle (β) is written:

$$I_g = \Phi_{b\beta} + \Phi_{d\beta} \quad (9)$$

Figure (2) shows the variation of the global solar radiation received by the flat surface of the solar collector and the powers absorbed respectively by the absorber and the transparent top cover (glass) as a function of the true solar time (TST).

It can be seen that the variation of solar radiation on the days of the calculations shows a sinusoidal profile marked by a minimum at sunrise and sunset and a maximum at solar noon.

It should be noted that, in general, the power absorbed by the absorber is always greater than that of the cover (glass). The power of the absorber directly influences the power of the glass and the power received by the heat transfer fluid (air), which will inevitably increase the temperature of the heat transfer fluid at the collector outlet.

It should be noted that at the start (before 6.30 a.m.), the power of the glass is greater than the power of the absorber, which is explained by the simple reason that the absorber is not yet active.

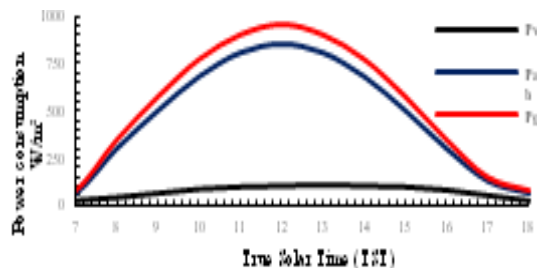


Fig.2: Variation of the global solar radiation received by the absorber and the glass cover (08/09/2021).

3.2. Variation of Ambient and Sky Temperatures

Several calculations were carried out on all working days; all curves have the same values except the default values of the measured values at the simulated one due to the metrological conditions. We notice that both temperatures have the same profile, the differences between the measured and simulated values are small and acceptable. The differences are generally due to the uncertainty of the measuring instruments used

in the experimental case and also to the simplifying hypotheses proposed during the numerical modelling and simulation.

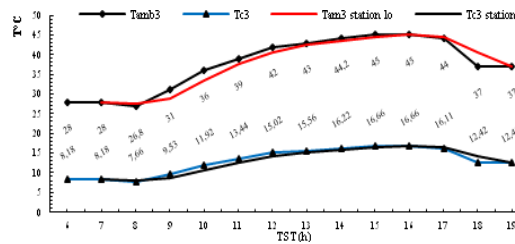


Fig. 3: Variation of ambient and sky temperatures with time (TST) (08/09/2021).

3.3. Temperature Variation of Different Sensor Elements

Fig. 4 shows the variation of measured and simulated temperatures of the different components of the solar collector and of the heat transfer fluid at the outlet. It should be noted that these curves are tight at the beginning of the system operation. This characterises the thermal inertia of the system. Once the thermal equilibrium is established, the differences between the measured and simulated values appear but are less important.

The experimental values of the temperatures of the heat transfer medium and the absorber show a rather large difference. This determines the efficiency of the type of material used and the quality of the heat transfer in our experimental system.

It should be noted that the temperature of the internal aluminium plate is higher than that of the fluid; this increase is probably due to the effect of favourable radiation from the solid than the fluid (air). The maximum value of the temperature of the fluid (air) that is obtained determines the feasibility of solar drying of the product. These values are very interesting and allow for forced or natural convection drying of ligaments and fruits especially for the period between 11:00 and 14:00 (TST).

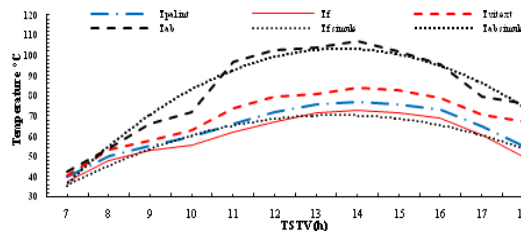


Fig. 4: Temperature variations of collector parts (experimental and simulated)

3.4. Variation of the Drying Air Temperature Inside the Drying Room

Figures (5, 6 and 7) show the variation of the temperatures at the sensor outlet and the average temperature taken at a distance of 400 mm from the air inlet in the drying room. It can be seen that the temperature variations evolve almost in the same way. This can be explained by the relationship between them. However, it can be seen that the differences between the two temperatures increase and become larger between 8 a.m. and 3 p.m., and then the difference decreases after 4 p.m. until it is almost zero. This is certainly due to the high intensity of solar radiation at the beginning and the lower intensity after 3 pm. In addition, after 16 h, this may also be due to the reduction in the amount of water in the form of moisture produced, which leads directly to a reduction in the thermal energy consumption of the drying air.

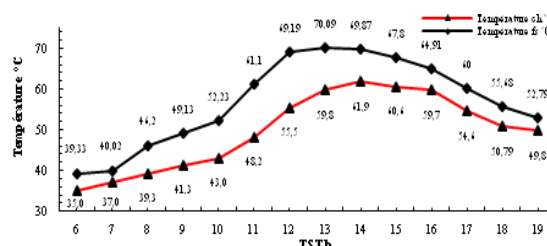


Fig. 5: Variation of temperatures at the outlet of the collector and inside the drying room, thickness $E_p=10\text{mm}$. 08/09/2021.

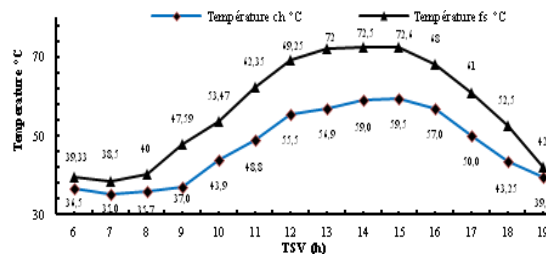


Fig. 6: Variation of temperatures at the outlet of the collector and inside the drying room, thickness $E_p=15\text{mm}$.
09/09/2021

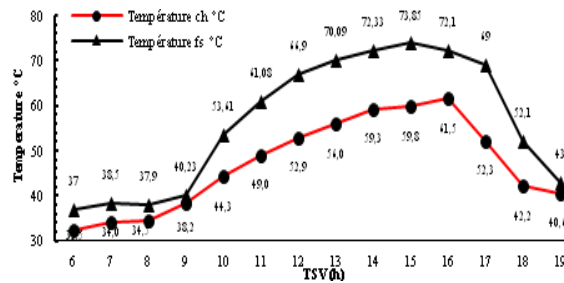


Fig. 7: Variation of temperatures at the outlet of the collector and inside the drying room, thickness $E_p=15\text{mm}$.
11/09/2021

3.5. Experimental Determination of the Drying Kinetics

The objective is to draw drying curves because these curves represent the variation of the water content (X) as a function of the drying time (t), and also the drying rate as a function of the water content as function of the drying time (t).

a- The thickness of the slices $E_p = 10 \text{ mm}$:

For tomato slices with a thickness of 10 mm, the final dry mass, with a total mass loss of 80%, is obtained after (10.5 h) of contained drying (see Fig.8). It should be noted that the product from the six racks did not dry at the same time. For the three control racks (1, 3 and 6) the total drying time was respectively (8h), (9h) and (10.5), (see Fig. 8). There is thus a gain in drying time.

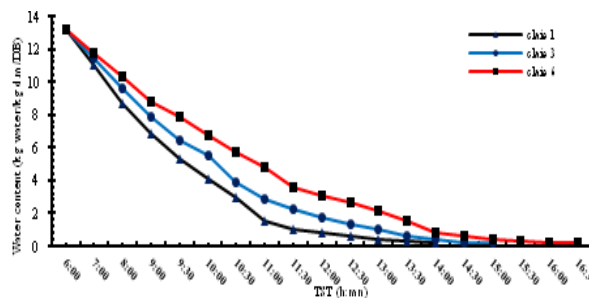


Fig. 8: Variation in water content of the dry base (thickness of 10 mm)

b- The thickness of the slices $E_p = 15 \text{ mm}$:

On the other hand, the washers of thickness $E_p=15\text{mm}$ dry differently because of the distance of the rack from the drying air inlet. It can be seen that the product in rack 1 dries and reaches its final water content after 10 hours of drying, whereas in rack 3 it took 11.5 hours of drying, and in the last rack it took almost 13 hours of drying (see fig.9). In this case, 13 hours of drying were necessary to reach favourable final dry base water content.

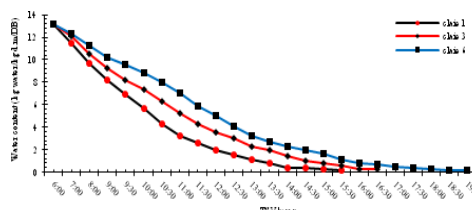


Fig.9: Variation in water content of the dry base (thickness of 15 mm).

c- The thickness of the slices $E_p = 20$ mm:

The analysis of the three curves (Fig. 10) allows us to see that they have almost the same curves as those presented in the previous figures (Fig.8 and Fig.9). It can be seen that the drying time has become more important because, for all the racks, the final dry base water content is obtained after more than 24 hours of drying, for the product of rack 1 is 27 hours of drying, for the product of rack 3 is 28.5 hours of drying for rack 6 is 29.5 hours of drying.

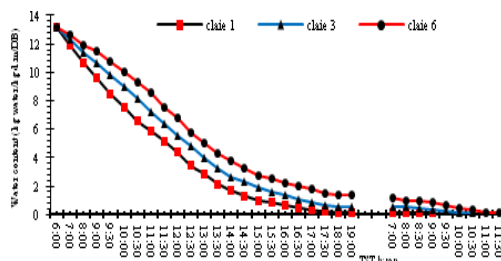


Fig.10: Variation in water content of the dry base (thickness of 20 mm).

3.6. Influence of Slice Size on the Quality of the Dried Product

During the drying process, the tomato slices dry with a water content of 10% for the 10 mm thick slices after 10.5 hours of drying, while the 15 mm thick slices dry after almost 13 hours of drying and 29.5 hours for the 20 mm thick tomato slices. It should be noted that for the three cases studied, firstly, for the 10 mm thickness, the slices are totally deformed and have taken on a very dark colour (see fig. 10) and have become fragile, which is unfavourable for storage, due to the large quantity of water extracted. Secondly, the 15 mm thick slice is partially deformed and has become dark and brittle (see fig. 11), which is favourable for storage. Thirdly, the 20 mm thick slice is less deformed (see fig. 12), which is very favourable for storage over long periods of time. The dark colour is due to the effect of the temperature of the heat transfer fluid (air), which has a negative influence on the product by degrading and reducing the amount of lycopene ($C_{40}H_{56}$) due to chemical reactions that degrade the colour and destroy the dietary fibres, as is the case here for the 10 mm thick slice, For the 15mm and 20 mm slice the product shows good results because the amount of heat exchanged between the slice and the fluid (air) is translated by the evaporation of water from the product with a slightly lower rate compared to the case of the 10mm thick slice.



Fig .10: Dried tomato, thickness of $E_p=10$ mm



Fig. 11: Dried tomato, thickness of $E_p=15$ mm



Fig.12: Dried tomato, thickness of $E_p=20$ mm

4. Conclusion

During the drying process, the influence of several parameters has been studied in order to choose the best drying conditions.

In the first phase of this study, we were interested in the thermal performance of the collector, which is the essential element of the drying process. It turns out that the efficiency of this element is very sensitive to variations in climatic parameters. The operating conditions considered in this study are very favourable. The exploitable daily time interval is very wide to justify solar drying in the Adrar region. The results showed that such a system with such performances could be used for an energy chain for solar drying of tomato and other vegetable products in the Adrar region

It has been shown that the use of indirect solar dryers has a great impact on the total drying time, and this is more noticeable when the dimensions of the product to be dried are large, as we have seen for slices with thicknesses of 15 mm and 20 mm.

The study of the drying kinetics of such a product through the parameters considered in this study, leads us to think of the possibility of a reduced time drying allowing preserving a product to consume it later with a very good quality which is not necessarily adapted to the conditions of drying at minimum time.

In conclusion, the drying process remains difficult to control because it depends largely on the climatic conditions and the physical characteristics of the materials of the different parts of the dryer and also the physic-chemical characteristics of the product to be dried.

In the future, we plan to extend this study to other applications such as the drying of other products with more complex structures like camel meat and Sidawn meat, as well as other local products with high production and consumption such as local dates, chilli, beans, chickpeas and beetroot.

References

- [1] N. MOUMMI et al, "Energy analysis of a solar air collector with rows of fins", *Renewable Energy*, Volume 29, Issue 13, October 2004, Pages 2053-2064
<https://doi.org/10.1016/j.renene.2003.11.006>
- [2] L. Adnane, "Contribution à l'étude des échanges convectifs en régime transitoire dans les Capteurs Solaires Plans à air ; Application au Séchage des produits agro-alimentaires.", Thèse, Université Biskra, 2012 ;
- [3] A. Labeled et al., "Etude théorique et expérimentale d'un capteur solaire plan à air muni d'une nouvelle forme de rugosité artificielle", *Revue des Energies Renouvelables* Vol. 12 N°4 (2009) 551 – 561 ;
- [4] B. TOUATI, "Etude théorique et expérimentale du séchage solaire des feuilles de la menthe verte (*Mentha viridis*)", Thèse, INSA de Lyon, Ecole Doctorale M.E.G.A, France, 2008 ;
- [5] B. H. Hassan, A. I. Hobani, "Thin layer drying of dates.", *Journal of Food Process Engineering*, vol. 23, pp. 177-189, 2000;
<https://doi.org/10.1111/j.1745-4530.2000.tb00510.x>
- [6] B.C. Boutaleb, "Etude Expérimentale du Séchage Convectif des Plantes Médicinales : Application à la Sauge et à la Verveine.", Thèse de D.E.S, Université Cadi Ayyad, Marrakech, Maroc, 1997 ;
- [7] Saadeddine MANA & all, "simulation of performance insoles plans for the development of solar field in Algeria.", *Energy Procedia* 18 (2012) 1220 – 1227;
<https://doi.org/10.1016/j.egypro.2012.05.137>
- [8] Aouès K. , Labeled A., Moumami A., Moumami N., Zellouf M, "Etude théorique et expérimentale d'un capteur solaire plan à air muni d'une nouvelle forme de rugosité artificielle.", *Revue des Energies Renouvelables* Vol. 12 N°4 (2009) 551 – 561 ;
- [9] S. MANA, "Analyse structurelle et conceptuelle des facteurs d'optimisation des performances des insolateurs plans munis d'ailettes pour des applications diverses en fonction des contextes géographiques et climatiques.", These, University, Biskra, Algeria; 2017

Nomenclature

X^* : the average water content of the product (kg water/kg dry weight)

X_{eq} : equilibrium thermodynamic water content determined by sorption isotherms

X_{cri} : the critical water content.

h_0 : the air-product heat transfer coefficient,

S_0 : the exchange surface between the product and the air at the initial instant,

$\Delta T=(T_s-T_h)$: the psychrometric deviation defined by the drying air conditions,

m_s : the dry mass of the product sample,

$L_v(T_h)$: the latent heat of vaporization of the product has the humid temperature of the drying air.

$\Phi_{b\beta}$ is the direct component, and $\Phi_{d\beta}$ is the diffuse component.